ELSEVIER

Global and Planetary Change 26 (2000) 445–465

GLOBAL AND PLANETARY CHANGE

www.elsevier.com/locate/gloplacha

Climate sensitivity to changes in land surface characteristics

Jacob O. Sewall [a,*], Lisa Cirbus Sloan [a], Matthew Huber [a], Scott Wing [b]

[a] *Department of Earth Sciences, University of California, Santa Cruz, CA 95064, USA*
[b] *Department of Paleobiology, Smithsonian Institute, Washington, DC, USA*

Received 10 December 1999; accepted 19 June 2000

Abstract

Using a recently developed global vegetation distribution, topography, and shorelines for the Early Eocene in conjunction with the Genesis version 2.0 climate model, we investigate the influences that these new boundary conditions have on global climate. Global mean climate changes little in response to the subtle changes we made; differences in mean annual and seasonal surface temperatures over northern and southern hemispheric land, respectively, are on the order of 0.5°C. In contrast, and perhaps more importantly, continental scale climate exhibits significant responses. Increased peak elevations and topographic detail result in larger amplitude planetary ~4 mm/day and decreases by 7–9 mm/day in the proto Himalayan region. Surface temperatures change by up to 18°C as a direct result of elevation modifications. Increased leaf area index (LAI), as a result of altered vegetation distributions, reduces temperatures by up to 6°C. Decreasing the size of the Mississippi embayment decreases inland precipitation by 1–2 mm/day. These climate responses to increased accuracy in boundary conditions indicate that "improved" boundary conditions may play an important role in producing modeled paleoclimates that approach the proxy data more closely.

Keywords: Cenozoic; paleoclimate; climate modeling; land surface; North America

1. Introduction

An ongoing goal for the paleoclimate modeling community is to reproduce global paleoclimate as accurately as possible. General circulation models (GCMs) are a commonly used tool in these endeavors. In order to assess the accuracy of GCMs, results from paleoclimate modeling experiments are often compared to the only available means of validation: climate estimates derived from proxy climate data. Physical, biological, and geochemical proxy data are frequently derived from limited localities, possibly representing areas as small as several square meters. Consequently, the information derived from proxy data reflects local and regional climate conditions in addition to the broader global climate overprint.

Fossils, the most common source of continental paleoclimate proxy data, are found in sedimentary rocks that formed predominantly in coastal lowlands and interior basins. Large-scale climatic conditions often differ from the prevailing regional conditions, especially in interior basins. Consequently, proxy data record local land surface characteristics as well as regional and global climates (Greenwood, 1992;

* Corresponding author. Tel.: +1-831-459-3504; fax: +1-831-459-3074.
E-mail address: jsewall@es.ucsc.edu (J.O. Sewall).

0921-8181/00/$ - see front matter
PII: S0921-8181(00)00056-4

Demko et al., 1998). For example, the species composition and structure of vegetation adjacent to streams and lakes is often markedly different from that found even a few hundred meters away from the water body. Vegetation close to fluvial or lacustrine depositional environments is more likely to be fossilized, and, therefore, paleoclimatic proxy data are likely to represent very local, in addition to regional or global, climate conditions.

This inherent bias in the proxy data makes comparisons to results from global-scale models difficult. Improved comparisons between model output and proxy data can be made by downscaling from the resolution of model output to the resolution of proxy data or through the application of regional climate models (e.g., Wilby et al., 1998; Sailor and Li, 1999; Reichert et al., 1999; Gebka et al., 1999). Unfortunately, the application of downscaling and regional modeling to paleoclimate investigations is in its infancy. Before either of these methods is attempted, it is important to have an accurate global climate simulation for the time interval in question — one that reproduces regional climates, as indicated by the proxy record, as accurately as possible. We can then either interpolate down from this global climate or use it to force a regional-scale model. With the objective of improving global paleoclimate simulations, we investigate the effects of land surface changes on the climate produced by a GCM. Specifically, we explore the influence that a more accurate global vegetation distribution and a more realistic topography (individual peaks and valleys, narrow mountain ranges, overall increase in topographic detail) have on model-produced climate.

An additional motivation for this work lies in a more historical context. In recent years, the spatial resolutions available in GCMs have increased greatly. However, it is not clear that researchers are taking full advantage of these resolution increases. When a new, higher resolution model version becomes available, a common practice is to interpolate old, low-resolution boundary conditions to new, higher resolutions.

For example, with the advent of Genesis version 2.0, researchers moved from an atmospheric and land surface resolution of spectral R15 ($\sim 4.5°$ latitude $\times$ 7.5° longitude) (e.g., Sloan and Rea, 1995) to an atmospheric resolution of spectral T31 ($\sim 3.75°$ latitude $\times$ 3.75° longitude) and a land surface resolution of 2° latitude $\times$ 2° longitude. When this resolution increase occurred, some researchers interpolated their R15 boundary conditions to the new, higher resolutions (e.g., Sloan and Pollard, 1998).

Topography at a low resolution, such as spectral resolution R15 or coarser, is highly smoothed. Individual peaks, valleys, and narrow mountain ranges are not resolved (Fig. 1A). Interpolating low resolution topography to a higher resolution (e.g., R15 topography interpolated to a resolution of 2° latitude $\times$ 2° longitude) generates the same highly smoothed topography, simply composed of more grid cells (Fig. 1B). It is possible that highly smoothed topography is a realistic enough boundary condition for simulations of global climate; however, it is equally possible that more realistic topography will influence model-produced climate in a way that produces a more accurate global paleoclimate.

There have been many previous studies that examined the impact of vegetation upon past climates (e.g., Bonan et al., 1992; Henderson-Sellers et al., 1993; Foley et al., 1994; Crowley and Baum, 1997). These studies were designed to gain a first-order estimate of the impact of a specific vegetation change upon climate. Our study focuses on the change in model-produced climate that occurs when the Eocene vegetation distribution is modified more subtly, based on our evolving knowledge of that distribution, rather than an investigation of extreme vegetation change.

Previous studies of the effect of topographic variation on climate changed topography globally by fixed amounts (e.g., Kutzbach and Gallimore, 1989), or changed elevations only for mountains that were fixed in location between the model cases (e.g., Sloan and Barron, 1992; Broccoli and Manabe, 1992; Kutzbach et al., 1993). In contrast, we explore the influence that increased topographic detail has on model-produced climate. Our global mean elevation varies little between cases, but maximum and minimum elevations increase and decrease, respectively. The locations of specific topographic features (e.g., highest and lowest points) change somewhat between cases. While the aforementioned studies focused on the effects that mountain evolution has on climate, our study is motivated by the question of accuracy in the portrayal of those mountains.

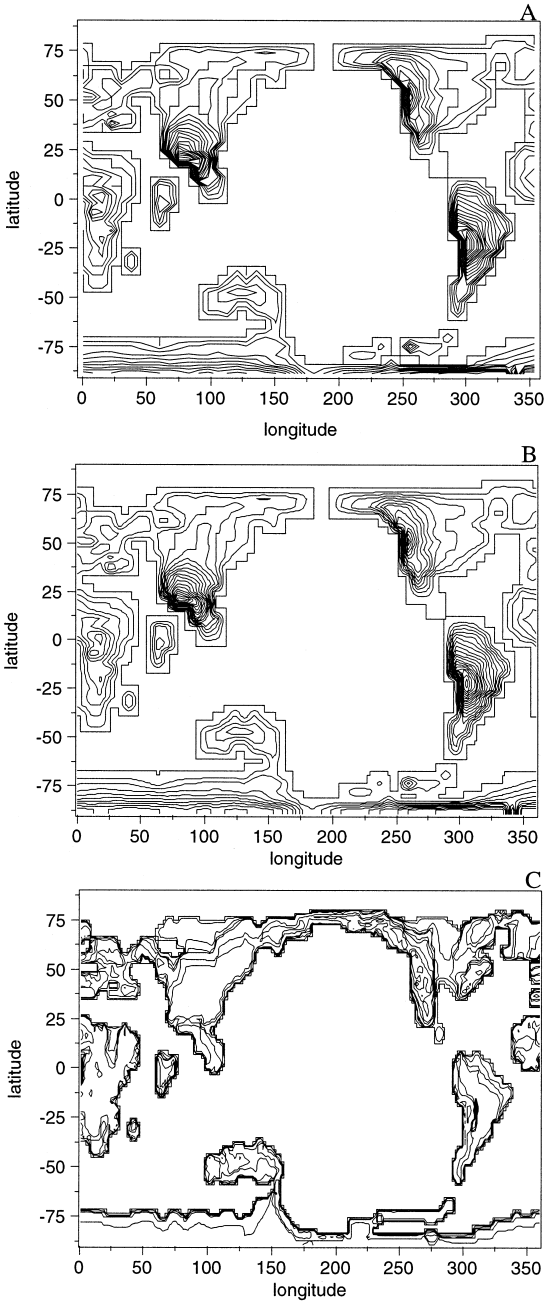

Fig. 1. (A) Old Eocene topography at spectral resolution R15 (~4.5° latitude×7.5° longitude), contours 0–2000 m at 100 m. (B) Old Eocene topography at a resolution of 2° latitude×2° longitude, contours 0–2000 m at 100 m. (C) New Eocene topography and shorelines at a resolution of 2° latitude×2° longitude, contours from 3800 to 600 m at 800 m, from 600 to 100 m at 250 m, from 100 to 10 m at 30 m, and 0 m.

2. Methods

Based on published elevation estimates, descriptions of regional tectonics, and geologic maps, we created new topographic and shoreline boundary conditions for the Eocene at a resolution of 2°×2° (Fig. 1C). We did this to include more detailed and realistic boundary conditions in our models. The old topographic and shoreline boundary conditions were a simple rendition of Early Eocene paleogeography that incorporated broad assumptions about locations of continental highlands and lowlands. The new topography was created region by region. First, elevation estimates and tectonic histories of prominent features were gathered (e.g., Molnar and Tapponier, 1975; Tapponier and Molnar, 1979; Plaziat, 1981; Molnar et al., 1987; Taylor et al., 1990; Roehler, 1993; Fitzgerald, 1994; Maxson and Tikoff, 1996; Allmendinger et al., 1997; Lamb and Hoke, 1997; Chorowicz et al., 1998; Gurnis et al., 1998). Then, based on knowledge of regional tectonics and possible maximum and minimum elevations, the shape and extent of mountain belts were created. Working from the major mountain belts and the tectonic framework of a region, topography was hand smoothed to sea level. For example, passive continental margins were given broader coastal plains than active continental margins. Lithospheric plate positions are modified from Scotese et al. (1988). Continental shorelines are based partially on global tectonics (e.g., Greenland had not rifted from Scandinavia (Scotese et al., 1988)) and partially on the location of contacts between Paleocene and Eocene sedimentary rocks as presented on various geologic maps.

In conjunction with the creation of a more realistic Eocene topography and orography, a more accurate global vegetation distribution was created. The vegetation distribution used in previous Eocene studies was constructed nearly 10 years ago and was based on limited paleobotanical information. The new Eocene global vegetation distributions were based on a larger database of macro- and microflora for the Early Eocene (e.g., Wing, 1998a,b; Rull, 1999; Wilf, 2000). In addition, the inferred influence of reduced latitudinal temperature gradients on global vegetation distributions was considered in this reconstruction.

In a trio of sensitivity studies, we investigate the effects of a more accurate vegetation distribution, more realistic, higher resolution topography, and changes in shorelines on Early Eocene climate.

3. Model

The model used in these studies is the Genesis climate model version 2.0 (Pollard and Thompson, 1995; Thompson and Pollard, 1997). This model reproduces present-day climate as well as other GCMs currently in use (Thompson and Pollard, 1997). The model contains a diurnal cycle and a full seasonal solar cycle. The atmospheric component of the model was run at a resolution of spectral T31 ($\sim 3.75°$ latitude $\times$ $3.75°$ longitude) with 18 vertical levels. The atmospheric component is coupled to a land surface with a resolution of $2° \times 2°$ (Pollard and Thompson, 1995). The vegetation was described using the 12 categories of Dorman and Sellers (1989). Clouds are predicted using prognostic three-dimensional water cloud amounts. Mixing ratios for the greenhouse gases CO_2, CH_4, N_2O, CFC_{11}, and CFC_{12} can be prescribed in the model, and the infrared radiation component of Genesis version 2.0 explicitly models the effects of greenhouse gases. Sea surface temperatures (SSTs) are prescribed.

4. Description of experiments

The control case for the trio of sensitivity studies, OLDVT, contains Eocene topography, shorelines, and vegetation distributions as defined in previous research efforts (boundary conditions are described in Sloan and Rea, 1995). Atmospheric carbon dioxide concentration was set at 300 ppm. Atmospheric CH_4 and N_2O concentrations were set at pre-industrial levels (0.700 and 0.285 ppm, respectively). The prescribed solar constant is the modern value of 1365 W/m^2. Soil is specified at the present global average (43% sand, 39% silt, 18% clay). The SSTs are zonally constant, seasonally varying SSTs that are characteristic of the warmest Cenozoic intervals. SST values were derived by fitting an energy balance model to a data set of Early Eocene SST interpretations and producing an annual average SST gradient and monthly zonal SST gradients (see full description and Fig. 1 in Sloan et al., in review). We use zonally constant SSTs because there are insufficient paleo-SST interpretations to allow characterization of longitudinal gradients in SST. The prescribed SSTs prohibit the development of El Nino/Southern Oscillation and other oceanic variability. Case OLDVT was started from the 16th year of an equilibrated Eocene run (control case of Sloan and Pollard, 1998) and run for 10 years.

The first sensitivity study focuses on the effect that a more accurate global vegetation distribution has on model-produced climate. This case is designated NEWVOLDT. With the exception of the new vegetation distribution (Fig. 2B), boundary conditions for NEWVOLDT are identical to those of OLDVT. NEWVOLDT was started from year 8 of OLDVT and run for 8 years.

The second sensitivity study investigates the effects of a more accurate, higher resolution topography and orography (Fig. 1C). This case is designated NEWVT. NEWVT uses the new topography and shorelines; all other boundary conditions are identical to NEWVOLDT. NEWVT was started from year 8 of OLDVT and run for 8 years. For each case, the final 3 years of results were averaged for analyses.

The third sensitivity study examines climate sensitivity of interior North America to a relatively small change in shoreline definition of the Mississippi embayment. This case is explained more fully below.

5. Results

5.1. Effect of vegetation changes upon Eocene climate

Because the only change between the NEWVOLDT and OLDVT cases is the inclusion of the new vegetation distribution, differences between the results of these two cases provide an assessment of the importance of vegetation specifications in modeling experiments. The vegetation distributions are quite different from each other (Fig. 2), however, the change in distributions has no significant effects on the mean global climate state. In December, January, and February (DJF), temperatures in the NEWVOLDT case are 0.51°C cooler over all land; Northern Hemisphere land is 0.18°C cooler and Southern Hemisphere land is 0.92°C cooler. In June, July, and August (JJA), the NEWVOLDT case is

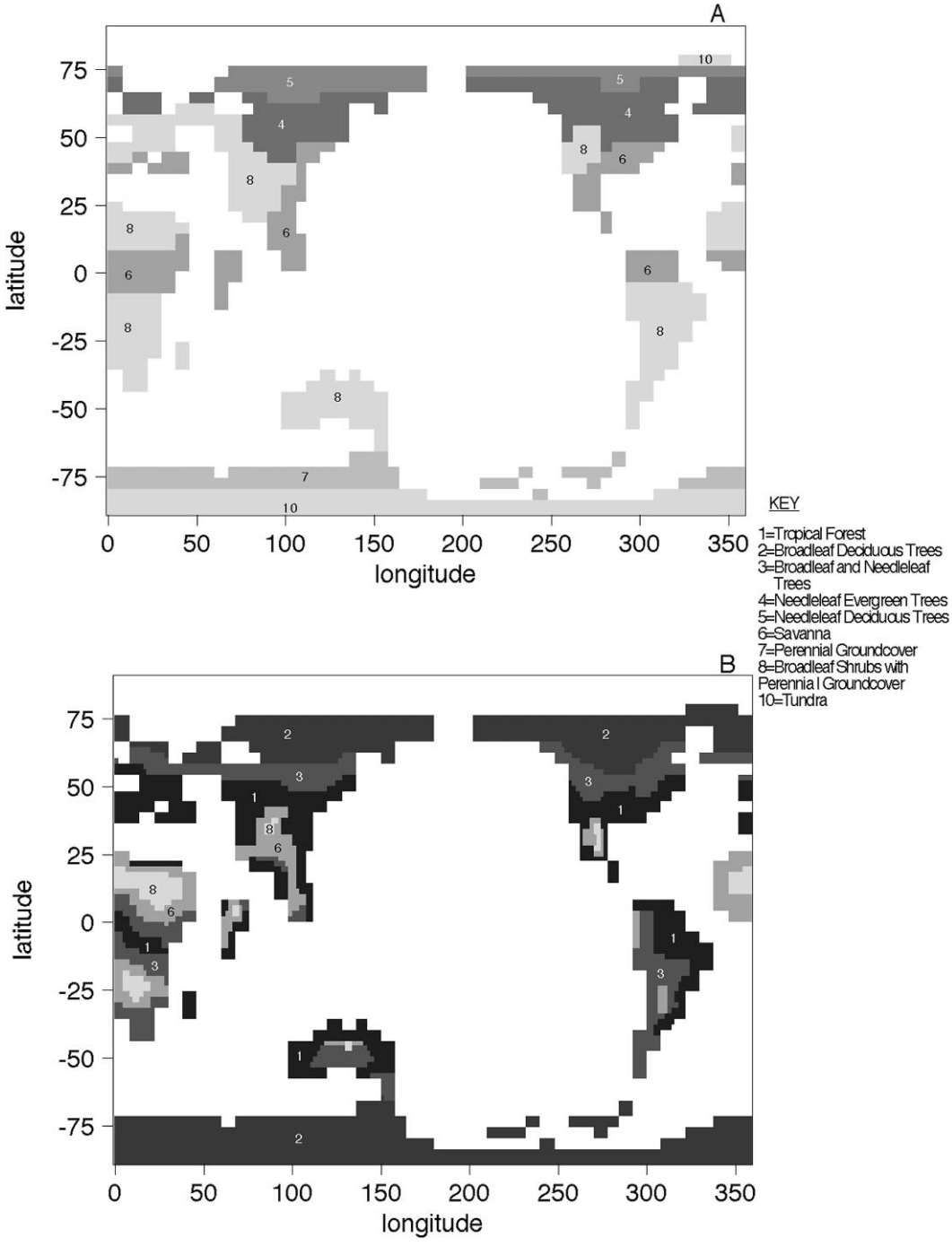

Fig. 2. (A) Old Eocene global vegetation distribution. (B) New Eocene global vegetation distribution. Vegetation categories are after Dorman and Sellers (1989).

0.64°C cooler over global land; Northern Hemisphere land is 0.86°C cooler while Southern Hemisphere land is 0.35°C cooler. Although the new vegetation distribution generates small responses in the global mean state, there are significant regional effects.

5.1.1. Surface temperatures

DJF surface temperatures decrease by 4°C over northern coastal Australia and regions of central South America and by 6°C over south, central Africa (Fig. 3A). In the NEWVOLDT case, surface temperatures in JJA are cooler by 4°C over central North

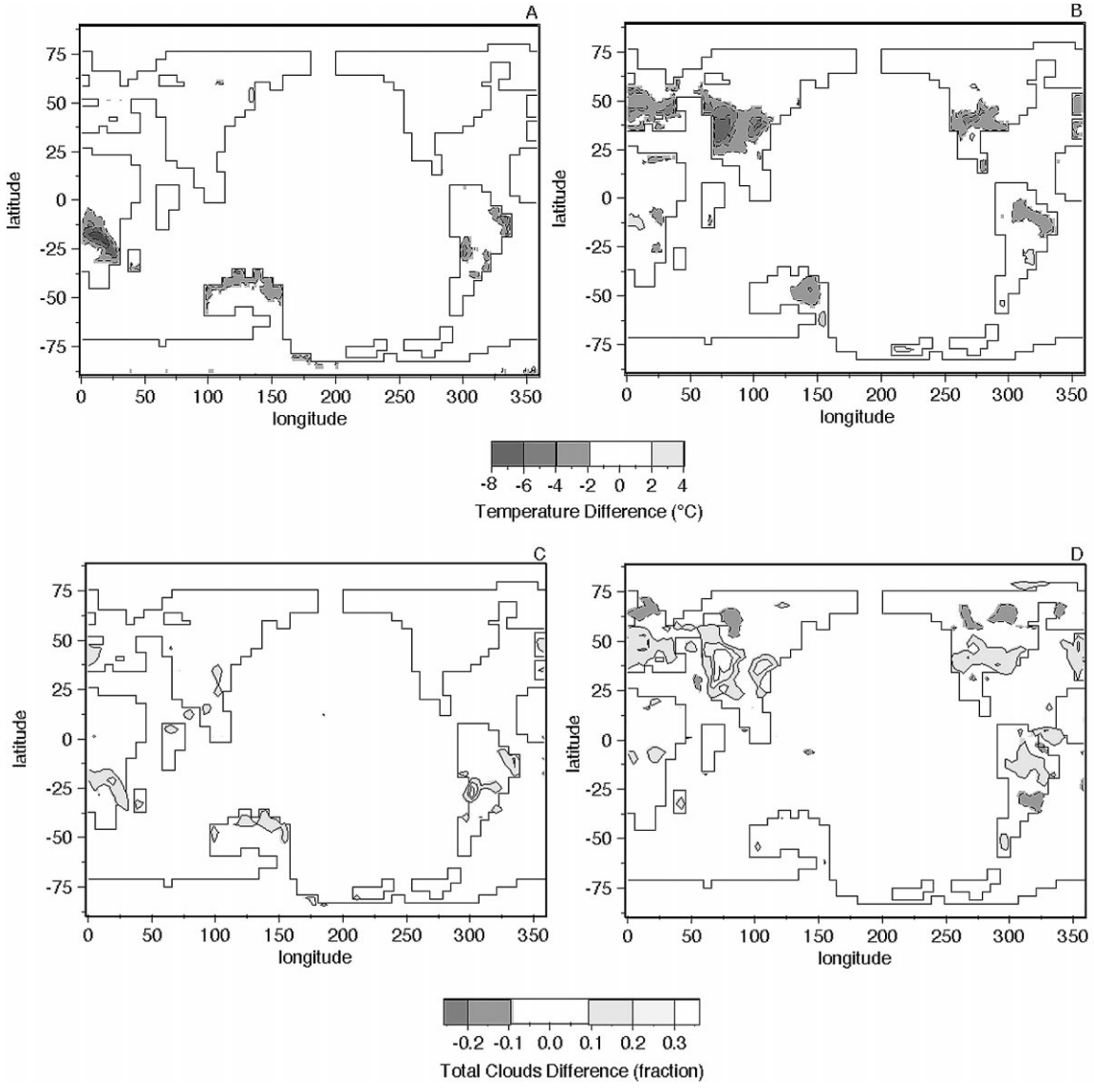

Fig. 3. (A) DJF surface temperature difference, NEWVOLDT minus OLDTV, contours from −8°C to 4°C at 2°C, no zero contour. (B) JJA surface temperature difference, NEWVOLDT minus OLDTV, contours from −8°C to 4°C at 2°C, no zero contour. (C) DJF total clouds difference, NEWVOLDT minus OLDTV, contours from −0.2 to 0.3 fraction at 0.1 fraction, no zero contour. (D) JJA total clouds difference, NEWVOLDT minus OLDTV, contours from −0.2 to 0.3 fraction at 0.1 fraction, no zero contour. All shaded differences shown on this plot are significant to the 99% level. Significance was calculated using Chervin and Schneider's *t*-test (Chervin and Schneider, 1976a,b).

America and central Australia and by 6°C over a large area of central Asia (Fig. 3B).

5.1.2. Total clouds

In DJF, the new vegetation generates a 20–30% increase in total cloudiness over central South America and an increase of 25% over south central Africa (Fig. 3C). Total cloudiness in the JJA NEWVOLDT case increases by 20–40% over central Asia and by up to 25% over north central South America and Europe (Fig. 3D).

5.1.3. Evapotranspiration

With the new vegetation, DJF evapotranspiration decreases by 2 mm/day over coastal regions of Asia. DJF evapotranspiration increases by 1–2 mm/day over central South America and north coastal Australia. Evapotranspiration increases over southern Africa and Southeast Asia for DJF are 2 mm/day.

Decreases in JJA evapotranspiration over the north coast of Africa are 1–2 mm/day with the new vegetation. An increase in JJA evapotranspiration of 1–2 mm/day is seen over central North America and evapotranspiration over Asia and central Africa increases by 2 mm/day.

5.1.4. Latent heating

In DJF, the new vegetation results in latent heating increases of up to 55 W/m^2 over most of South America (Fig. 4A). DJF latent heating increases of up to 30 W/m^2 are found over north coastal Australia, parts of Southeast Asia, and much of southern and central Africa (Fig. 4A). Latent heating in JJA increases by up to 55 W/m^2 over regions in central Africa and central Asia (Fig. 4B).

5.2. New topography and shorelines vs. old topography and shorelines

The two different topographies presented here represent changes in knowledge about the Eocene land surface. Because the only change between the NEWVOLDT and NEWVT cases is the inclusion of the new topographic and shoreline boundary conditions, differences between these two cases provide an assessment of the importance of "realistic" topography for our modeling experiments.

5.2.1. Elevation differences

Despite the fact that the global mean elevations of the two topographies are very similar, there are significant differences between the old and new topographies on almost every continent (Fig. 5). Global mean elevation of the old topography is 137.43 m and the global mean elevation of the new topography is 141.28 m. Elevation increases of note in the new topography are found over the North American Cordillera, the Appalachian Mountains, the Andes, parts of Southeast Asia, the Transantarctic Mountains, and rift shoulders of India and Greenland (Fig. 5). Elevation decreases of note are associated with the proto Altiplano, the South American Foreland, and the proto Himalayas. The most significant shoreline changes are the addition of Beringia connecting North America and Asia and an increase in the size of the Mississippi embayment (Fig. 5).

5.2.2. Surface temperatures

Because shorelines were changed between NEWVOLDT and NEWVT (Fig. 1B,C), surface temperature differences between the two cases are masked to remove points that have changed from land to sea and vice versa. These experiments have fixed SSTs and, therefore, surface temperature differences in those regions are meaningless.

Over the North American Cordillera, mean annual temperature (MAT) decreases by up to 16°C (Fig. 6A). Decreases in MAT of 5–10°C occur over the Appalachian Mountains, the Andes, the Transantarctic Mountains, parts of Southeast Asia, a few areas in central Australia, and rift shoulders of India and Greenland (Fig. 6A). MAT over central Africa and portions of the proto Himalayas increases by 5°C or more (Fig. 6A) in the NEWVT case. MAT over the South American Foreland is up to 10°C higher in the NEWVT case.

Seasonal differences in surface temperature between the old and new topographies largely reflect the same pattern as differences in MAT (Fig. 6A,B,C). In both DJF and JJA, there is cooling of up to 16°C over the North American Cordillera and cooling of 5–10°C is seen over the Appalachian Mountains, the Andes, the Transantarctic Mountains, and rift shoulders of India and Greenland (Fig. 6B,C). In both DJF and JJA, there is warming of up to 10°C

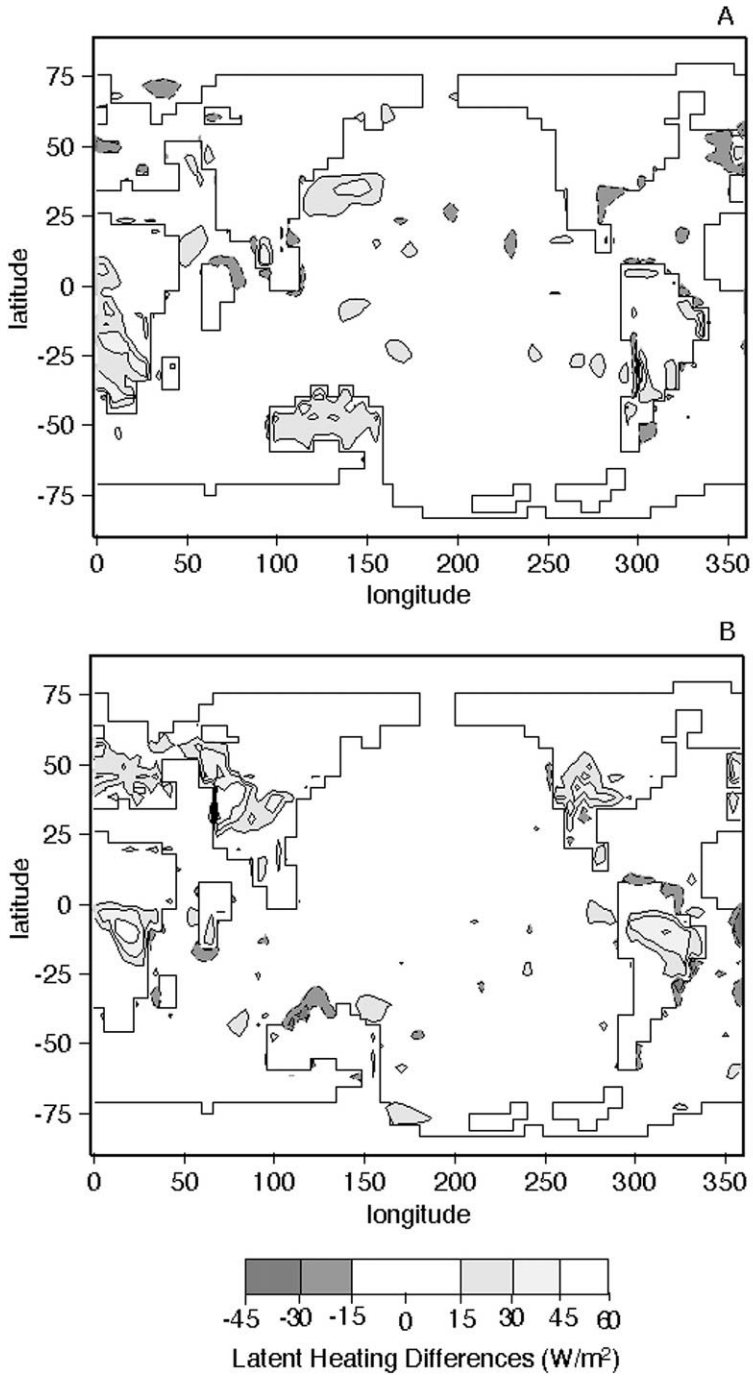

Fig. 4. (A) DJF latent heat difference, NEWVOLDT minus OLDTV, contours from -45 to 60 W/m^2 at 15 W/m^2, no zero contour. (B) JJA latent heat difference, NEWVOLDT minus OLDTV, contours from -45 to 60 W/m^2 at 15 W/m^2, no zero contour. All shaded differences shown on this plot are significant to the 99% confidence level. Significance was calculated using Chervin and Schneider's *t*-test (Chervin and Schneider, 1976a,b).

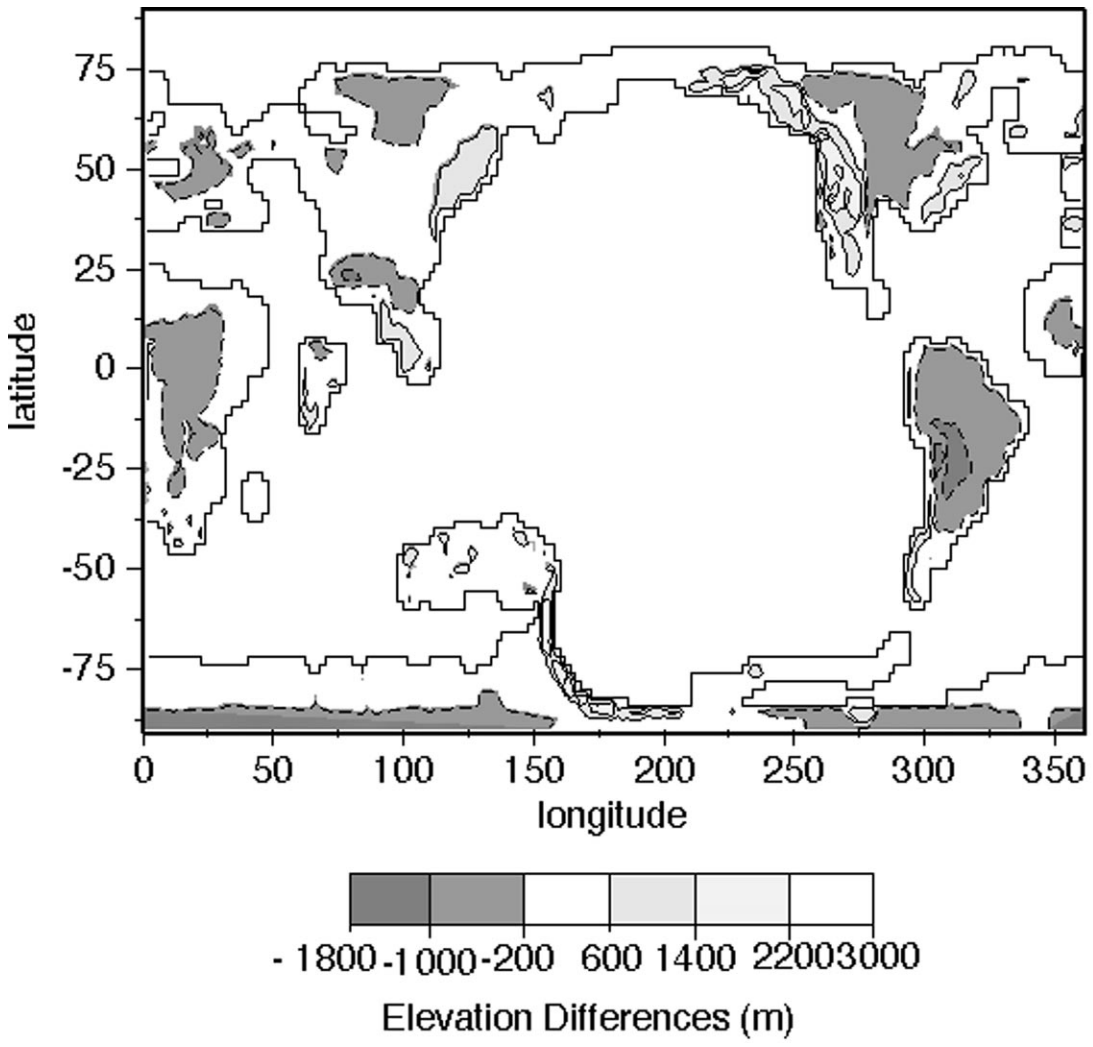

Fig. 5. Topography differences, new Eocene topography at $2° \times 2°$ minus old Eocene topography at $2° \times 2°$. Contours from -1800 to 3000 m at 800 m.

over the proto Altiplano and South American Foreland, 5–10°C of warming over the proto Himalayas, and increases of up to 5°C over central Africa (Fig. 6B,C). The only seasonal surface temperature changes of note are found over the interior of North America. In DJF, interior North America is 5–15°C cooler with the new topography (Fig. 6B). In JJA, the foreland region of western interior North America warms by over 5°C (Fig. 6C).

5.2.3. Five hundred millibar winds

In the upper atmosphere of the NEWVT case, an enhanced trough and ridge structure is apparent over the mid to high latitude Northern Hemisphere in DJF, but is less pronounced in the Southern Hemisphere (Fig. 7A,B). The enhanced trough and ridge structure is especially pronounced in JJA over the mid to high latitude Northern Hemisphere and around the Transantarctic Mountains and the "Australian Neck" in the Southern Hemisphere (Fig. 7C,D).

5.2.4. Surface winds

DJF northerlies over southern Alaska are replaced by southerlies in NEWVT. Southwesterly DJF flow over western, coastal North America is replaced by southerlies (Fig. 8A,B). In JJA, the new topography

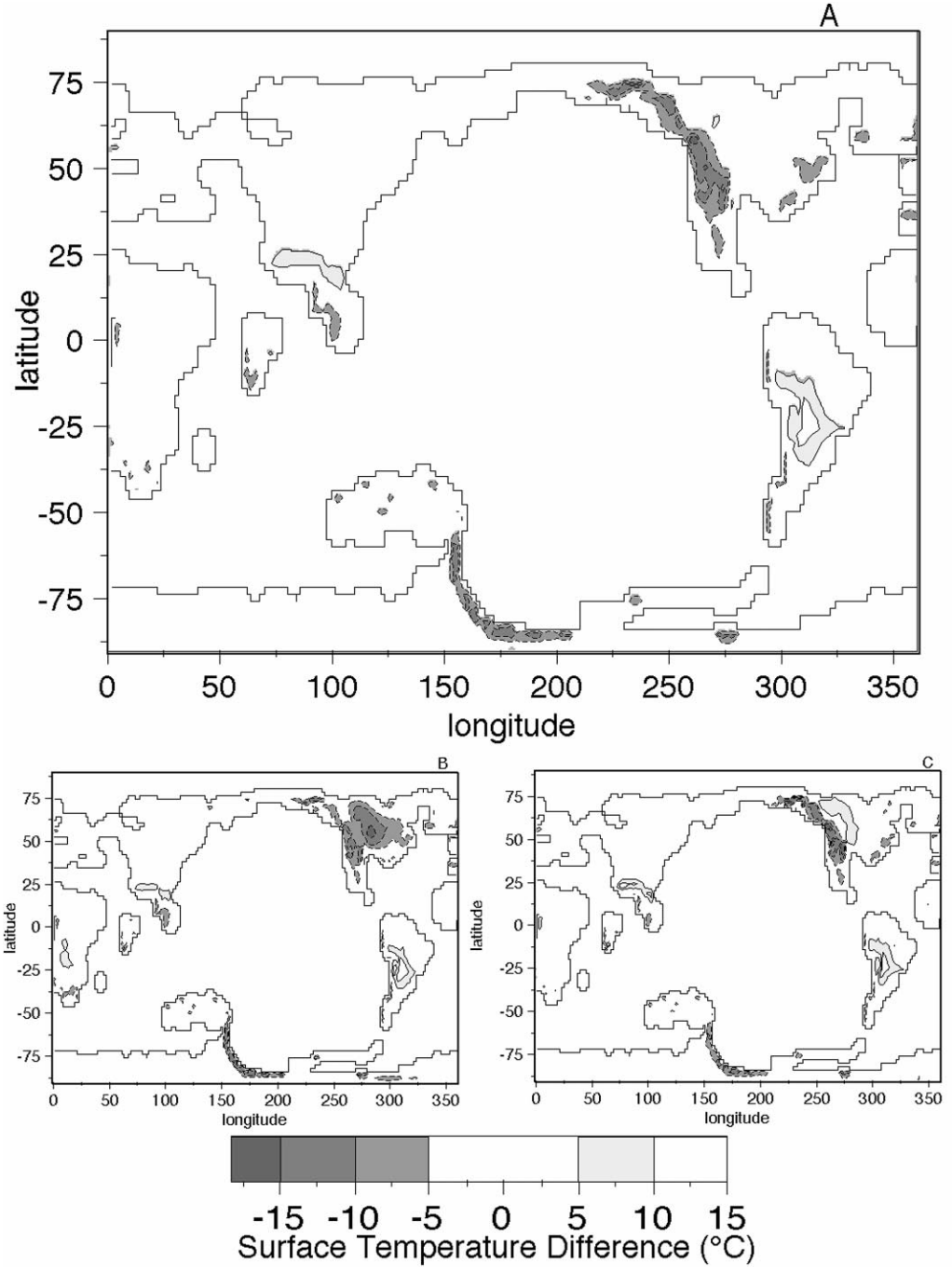

Fig. 6. (A) MAT difference, NEWVT minus NEWVOLDT. (B) DJF surface temperature difference, NEWVT minus NEWVOLDT. (C) JJA surface temperature difference, NEWVT minus NEWVOLDT. Contours for all plots are from −20°C to 15°C at 5°C, no zero contour. All differences shown on this plot are significant to the 99% confidence level. Significance was calculated using Chervin and Schneider's *t*-test (Chervin and Schneider, 1976a,b).

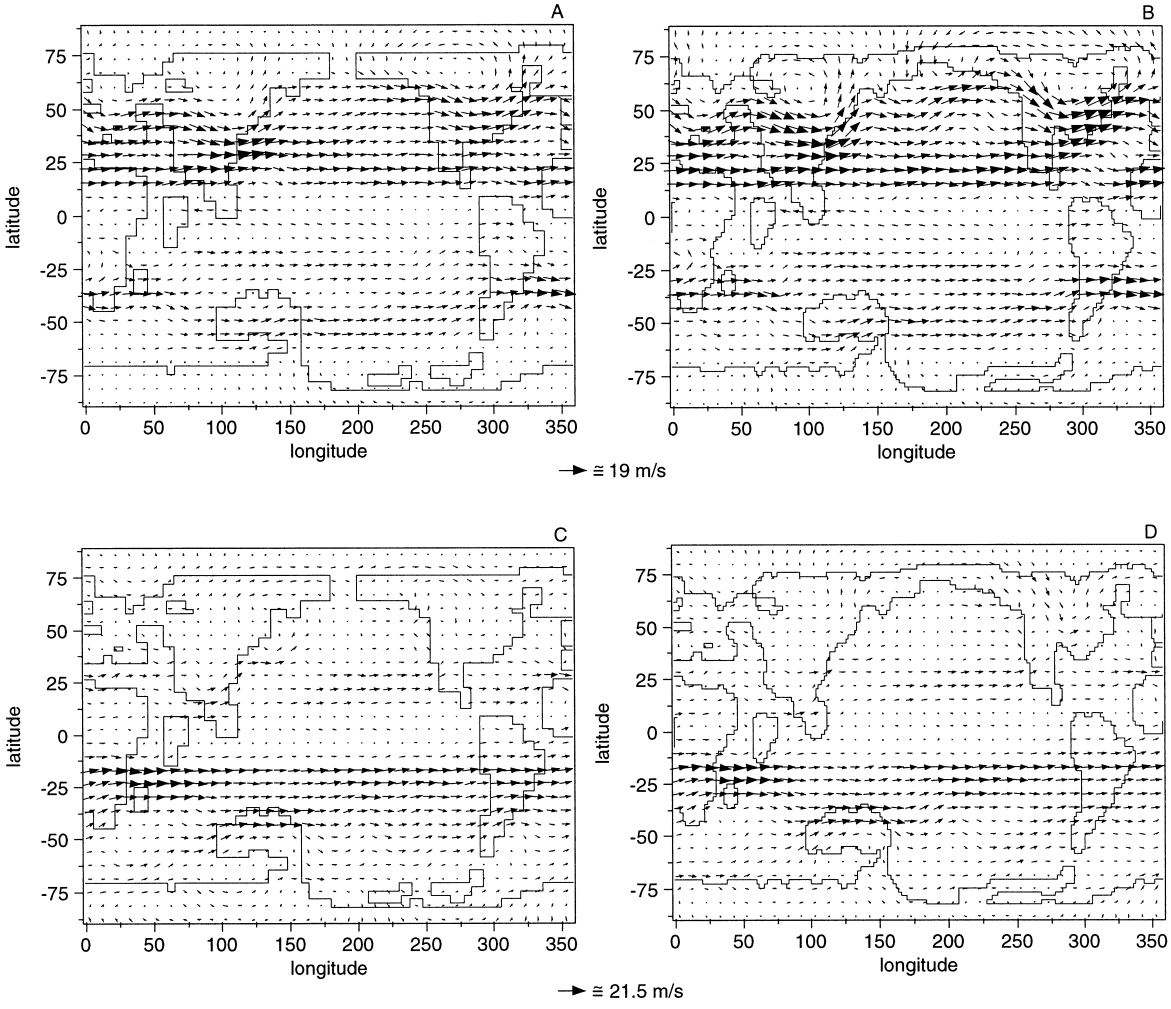

Fig. 7. (A) NEWVOLDT DJF 500 mbar winds, (B) NEWVT DJF 500 mbar winds, (C) NEWVOLDT JJA 500 mbar winds, D) NEWVT JJA 500 mbar winds.

weakens westerly flow over Southeast Asia (Fig. 8C,D). The northerlies in JJA over central North America are stronger and easterlies are introduced over the front of the Cordillera . JJA southerlies over the Mississippi embayment are strengthened in the NEWVT case (Fig. 8C,D).

5.2.5. Sea level pressure

The DJF sea level pressure patterns generated with the old and new topographies are very similar in the Southern Hemisphere, with the magnitude of sea level pressure associated with the new topography being slightly lower than that with the old topography (not shown). The only Southern Hemisphere area where DJF sea level pressure with the new topography exceeds that with the old topography is immediately offshore of the Transantarctic Mountains. In NEWVT DJF Northern Hemisphere sea level pressure, the high over Asia is stronger and penetrates farther north. In DJF, the Aleutian low is stronger but restricted to Beringia. A large winter high occurs over central North America and a low has replaced the high over the Labrador strait (not shown).

In JJA, sea level pressure is significantly lower with the new topography over central Siberia, north

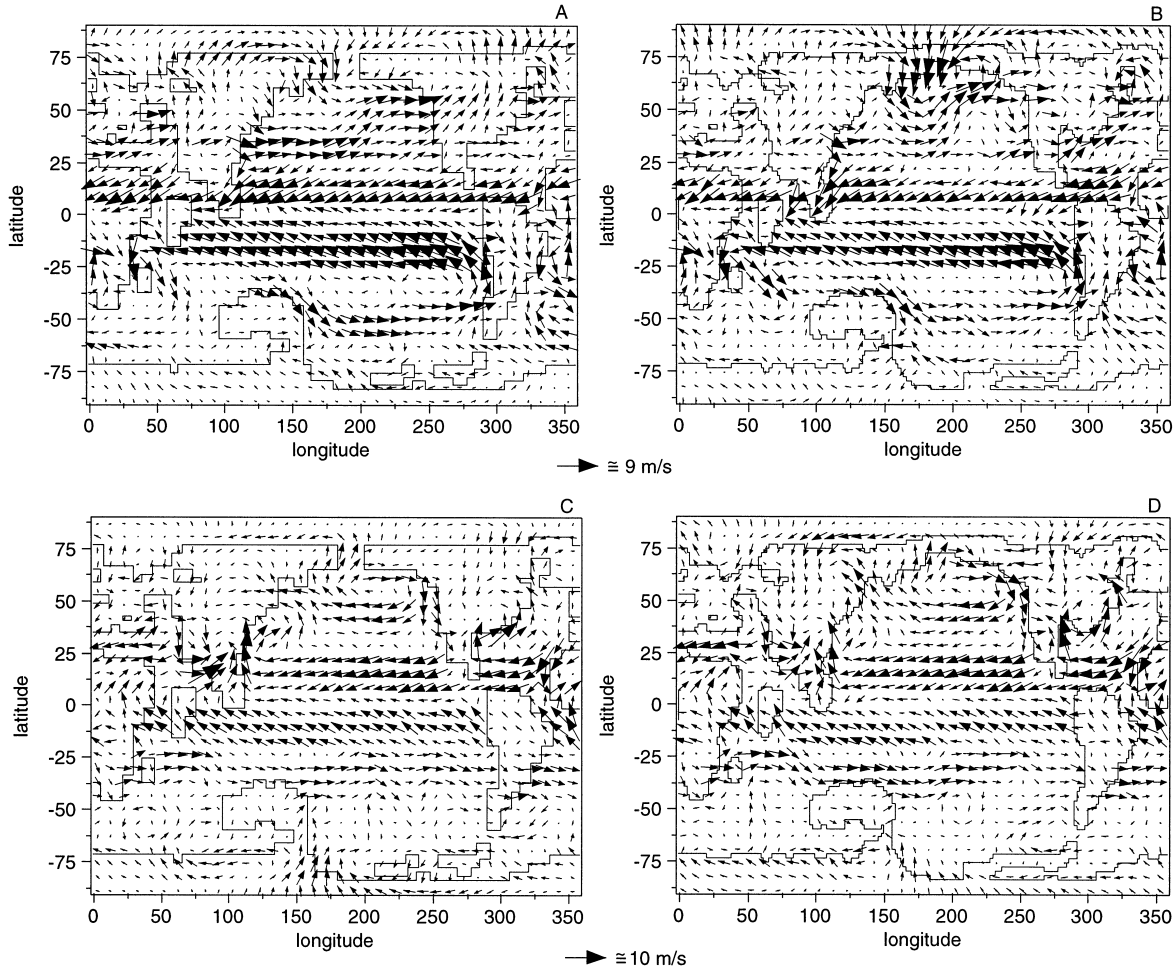

Fig. 8. (A) NEWVOLDT DJF surface winds, (B) NEWVT DJF surface winds, (C) NEWVOLDT JJA surface winds, (D) NEWVT JJA surface winds.

central North America, the North American Cordillera, Australia, and portions of Antarctica (not shown). JJA sea level pressure is higher over south central North America and off the east coast of South America. In JJA, the low over Asia is stronger and extends farther north. The Aleutian high is slightly stronger. With the new topography, there is a summer low over the North American Cordillera and a high over east central North America (not shown).

5.2.6. Convective precipitation

DJF convective precipitation with the new topography decreases by 3 mm/day over central Africa and by 2–4 mm/day over the South American Foreland. Just north of the South American Foreland, however, DJF convective precipitation increases by 2 mm/day (Fig. 9A). In DJF, convective precipitation increases by up to 6 mm/day over the southern coast of Alaska and by 4 mm/day over western and southeastern North America (Fig. 9A).

JJA convective precipitation decreases by 3 mm/day along the west coast of North America and by 7–9 mm/day in the proto Himalayan region. The new topography generates JJA convective precipitation increases of 3 mm/day northeast of the proto Himalayas and by 2 mm/day along the east coast of China (Fig. 9B). In JJA, convective precipitation increases by 3–5 mm/day over the proto Front

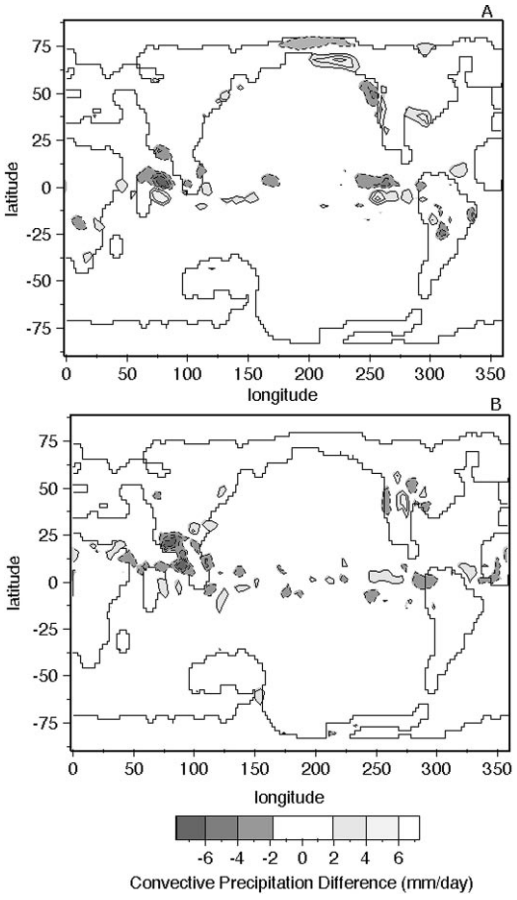

Fig. 9. (A) DJF convective precipitation difference, NEWVT minus NEWVOLDT, contours from −8 to 8 mm/day at 2 mm/day, no zero contour. (B) JJA convective precipitation difference, NEWVT minus NEWVOLDT, contours from −8 to 8 mm/day at 2 mm/day, no zero contour. All shaded differences shown on this plot are significant to the 99% confidence level. Significance was calculated using Chervin and Schneider's *t*-test (Chervin and Schneider, 1976a,b).

Ranges of North America and by 2 mm/day over central North America (Fig. 9B).

5.2.7. Convective clouds

In the DJF NEWVT results, convective cloudiness decreases by up to 50% over the proto Front Ranges and into central North America. Convective cloudiness decreases by 30% over the South American Foreland.

In the NEWVT case, there is a 30% decrease in JJA convective cloudiness at the base of the West Antarctic Peninsula. JJA convective cloudiness decreases by 40% over central and northern North America and by 10–30% over west central South America. With the inclusion of the new topography, JJA convective clouds increase by 30% off the west coast of North America and by 30–40% over the Mississippi embayment and the proto Front Ranges of North America.

6. Discussion

6.1. Climate sensitivity to changes in the global vegetation distribution

Significant responses to changes in the global vegetation distribution are limited to the regional-scale; this is an important result given that proxy data reflect regional, as well as global, climate conditions. The most significant responses to our specified vegetation changes are regional increases in evapotranspiration, which in turn generate increases in clouds and latent heating, and decreases in incoming radiation, and surface temperature. As leaf area index (LAI) is the vegetation characteristic that most influences evapotranspiration in the model and because responses are found predominantly in areas where vegetation has been altered from shrublands to tropical forests (Figs. 2–5) (a substantial increase in LAI), we hypothesize that the climatic changes outlined above are related to increases in LAI.

If the LAI of each vegetation type, as defined in the climate model, is multiplied by the areal extent of that vegetation type, the result is the areal equivalent leaf area. The new vegetation distribution has a substantially greater leaf area equivalent in both DJF and JJA, 1.18×10^8 and 1.49×10^8 km^2 greater, respectively (Table 1). We find that these LAI changes have the greatest climatic impact in midlatitudes of the summer hemisphere.

The increase in LAI results in a corresponding increase in evapotranspiration . This is seen most clearly over central Asia and interior North America in JJA and over Africa around 25° south latitude, along the northern coast of Australia, and in areas of South America in DJF. The increased evapotranspiration has a direct effect on surface temperature,

Table 1
LAI of each of the included Dorman and Sellers (1989) vegetation types multiplied by the areal extent of that vegetation type in the old and new vegetation distributions

Vegetation type	LAI × areal extent in old vegetation distribution (km^2)	LAI × areal extent in new vegetation distribution (km^2)	Difference in coverage (new minus old) (km^2)
(A) JJA			
1 (Tropical forest)	0	2.16×10^8	2.16×10^8
2 (Broadleaf deciduous trees)	0	7.90×10^7	7.90×10^7
3 (Broadleaf and needleleaf trees)	0	1.41×10^8	1.41×10^8
4 (Needleleaf evergreen trees)	1.58×10^8	0	-1.58×10^8
5 (Needleleaf deciduous trees)	1.72×10^7	0	-1.72×10^7
6 (Savanna)	1.10×10^8	6.76×10^7	-4.24×10^7
7 (Perennial groundcover)	2.64×10^6	0	-2.64×10^6
8 (Broadleaf shrubs with perennial groundcover)	7.13×10^7	6.83×10^6	-6.45×10^7
9 (Broadleaf shrubs with bare soil)	0	0	0
10 (Tundra)	1.63×10^6	0	-1.63×10^6
Total	3.61×10^8	5.10×10^8	1.49×10^8
(B) DJF			
1 (Tropical forest)	0	2.16×10^8	2.16×10^8
2 (Broadleaf deciduous trees)	0	3.85×10^7	3.85×10^7
3 (Broadleaf and needleleaf Trees)	0	1.01×10^8	1.01×10^8
4 (Needleleaf evergreen trees)	1.34×10^8	0	-1.34×10^8
5 (Needleleaf deciduous trees)	0	0	0
6 (Savanna)	7.13×10^7	4.6×10^7	-2.5×10^7
7 (Perennial groundcover)	1.66×10^7	0	-1.66×10^7
8 (Broadleaf shrubs with perennial groundcover)	6.78×10^7	1.08×10^7	-5.70×10^7
9 (Broadleaf shrubs with bare soil)	0	0	0
10 (Tundra)	4.31×10^6	0	-4.31×10^6
Total	2.94×10^8	4.12×10^8	1.18×10^8

The table was split into seasons because the LAI of deciduous trees varies seasonally. LAI multiplied by areal extent of vegetation type peaks in JJA because that is Northern Hemisphere summer. Deciduous trees have their greatest LAI in the summer. The Northern Hemisphere has a greater land area than the Southern Hemisphere and thus supports more vegetation. Consequently, the season in which Northern Hemisphere deciduous trees have their leaves will have greater overall vegetative cover than the season in which Southern Hemisphere deciduous trees have their leaves.

cooling it by 2–6°C in these areas (Fig. 3). These changes are the inverse of those seen when LAI and fractional cover are decreased by changing tropical rainforest to savanna (Crowley and Baum, 1997).

The increased evapotranspiration in our model has an additional, indirect effect on surface temperature. The increase in evapotranspiration provides more moisture for clouds (Fig. 3A,B); as clouds form, latent heat is released. Latent heat and total cloudiness increase over central Asia, interior North America, Africa around 25° south latitude, the north coast of Australia, and regions of South America in the summer (Figs. 3A,B and 5A,B). The increased cloudiness decreases incoming solar radiation by up to 80 W/m^2 (not shown) and there is a consequent summer cooling in these regions.

Based on this series of modeled feedbacks, it appears that LAI is the most important vegetation characteristic influencing climate. Vegetation changes are, therefore, only climatologically significant where there is a substantial change in LAI. It should be noted that this response is dependent on the operational definition of vegetation in our model; in other climate models, depending on the vegetation parameterizations, the effects of vegetation change on climate may be different. The sensitivity of cli-

mate to changes in the global vegetation distribution may also change with different vegetation parameterization schemes.

6.2. Climate sensitivity to changes in topography

Surface temperature changes in NEWVT, as compared with NEWVOLDT, are, for the most part, directly associated with regions of elevation change (Figs. 6 and 7). In regions where elevation increased, surface temperature decreased and vice versa. When change in model-produced MAT is plotted against the difference in elevation between the two topographies, it is found that temperature decreases by 6.1°C for every kilometer increase in elevation (Fig. 10). This is very close to the moist adiabatic lapse rate of 6.5°C/km. Cooler temperatures in areas such as the North American Cordillera and warmer temperatures in areas including the South American Foreland are almost entirely a direct effect of the elevation change in those areas.

Model output from NEWVT does not match proxy data estimates of Early Eocene MAT (e.g., MAT in the Rocky Mountains is from −8 to −3°C in NEWVT, proxy data estimates of MAT for the same area are 9–24°C (Wing and Greenwood, 1993; Greenwood and Wing, 1995)). This is probably because proxy data are most likely to be preserved in intermontane basins, and a 2° × 2° land surface resolution is too coarse to resolve these basins that most likely occur at a scale smaller than 40,000 km^2 (Fig. 11). Instead, these basins are represented as part of a broad mountain feature. Consequently, the elevation of these fossil locales is overestimated in the model, and MAT in these regions is underestimated.

If the basin elevation where the abovementioned proxy data were deposited is assumed to be ~750 m above sea level (Greenwood and Wing, 1995) and the 2° × 2° model elevation is ~3000 m (Fig. 1C),

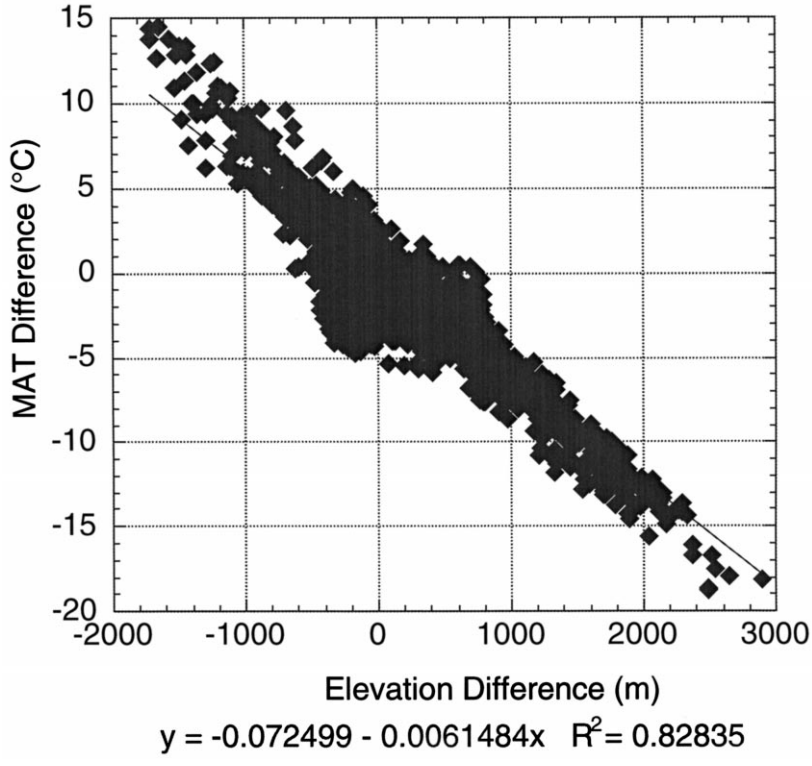

Fig. 10. MAT difference (NEWVT minus NEWVOLDT) vs. elevation difference (new Eocene topography minus old Eocene topography). Line slope is −6.15°C/km.

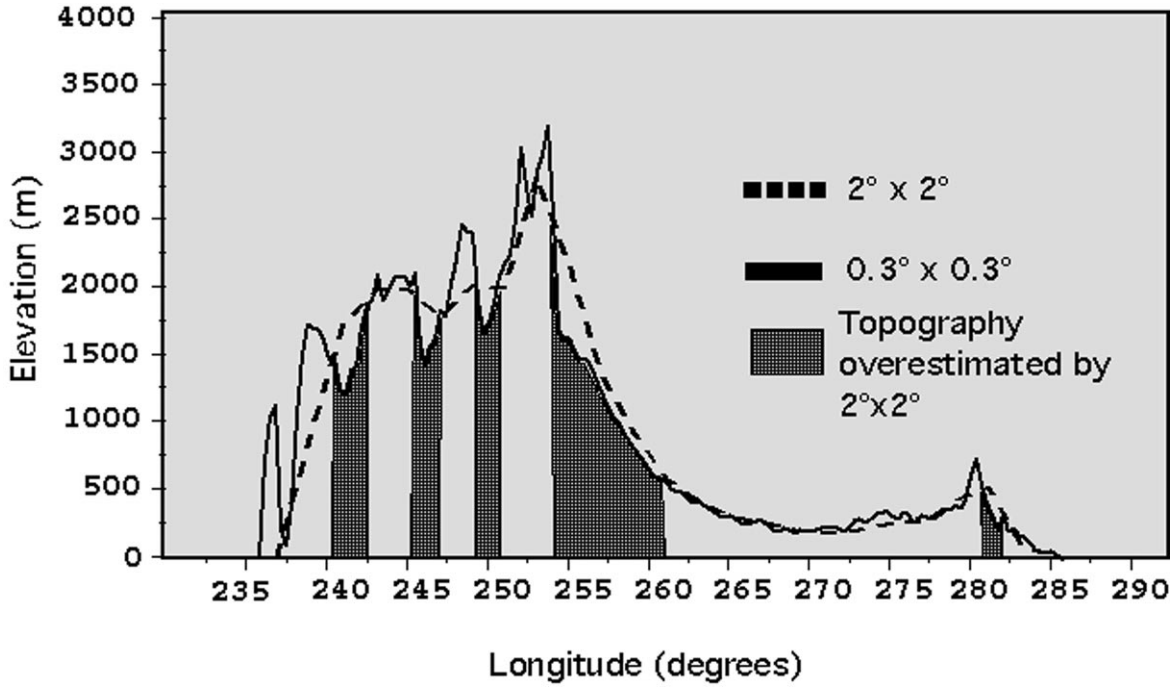

Fig. 11. Cross section of present day North America at 40° north latitude. Topography at a resolution of $2° \times 2°$ over topography at a resolution of $0.3° \times 0.3°$.

the elevation difference is 2250 m. Thus, the model calculates air temperature for air at an elevation 2250 m higher than the actual elevation of that parcel of air. If a moist adiabatic lapse rate of -6.5°C/km is applied, the model-calculated air temperature will be 14.6°C lower than the actual temperature of that parcel of air. If the model-calculated air temperature is corrected for the lapse rate effect (add 14.6°C to the model-produced temperature), MAT results from NEWVT become 7–12°C, much closer to the proxy data estimates of MAT.

As has been previously stated, surface temperature differences of up to 18°C (Fig. 6) are generated by the new topography. These surface temperature differences are wholly attributable to gross subgridscale parameterizations (lapse rate, specifically). The magnitude of these differences is so large that subtler surface temperature differences driven by more dynamic, explicitly defined processes (e.g., advection, convection, and radiation) are eclipsed. Better correlation of model output and proxy data will require much higher land surface resolutions, a more sophisticated downscaling approach than simply utilizing the atmospheric lapse rate, or a combination of both.

The decreased MATs as a result of increased elevation are responsible for perennial snow in the North American Cordillera and the Transantarctic Mountains in the NEWVT case (not shown). Snowfall rate (not shown) increases substantially over the North American Cordillera in DJF. There are no significant changes in snowfall rate over JJA Antarctica. Snow falls only in the winter hemisphere; however, summer temperatures are cool enough in isolated regions (not greater than one grid cell in area) for snow to be present year round. The areas of perennial snow are in equilibrium with the climate; the areal extent of the snowpack has not changed for the last 4 years of the model run. For the North American Cordillera, the presence of Eocene snow pack is possibly supported by isotopic signatures in sediments of the Green River Formation (Dettman and Lohmann, 1993, 2000; Norris et al., 1996).

For the most part, seasonal changes in temperature mirror the changes in MAT and are directly related to the changes in elevation. The only signifi-

cant changes in seasonal surface temperature that are not directly related to changing elevation are found over central North America. In JJA, a 5°C warming over the northern foreland of North America (Fig. 6C) is linked to changes in incoming solar radiation. With the inclusion of the new topography, total clouds in JJA decrease by 40% (not shown) in this region. Consequently, incoming solar radiation received at the surface (not shown) increases by 60–120 W/m^2. This generates summer warming of 5°C. In DJF, the presence of a large high-pressure system, and the associated trough, brings Arctic air as far south as the Mississippi embayment (Figs. 7B and 9B). The result is a cooling of up to 15°C relative to the NEWVOLDT results, which have much more zonal winter winds, and, therefore, less continental interior penetration of Arctic air (Figs. 6B and 8A). This enhanced trough and ridge structure of the upper atmosphere that is responsible for DJF cooling in North America is an expected result of increasing elevation and roughness of the topography. Other researchers (e.g., Kutzbach et al., 1993; Ruddiman and Prell, 1997) have noted similar responses.

The primary effect of the enhanced trough and ridge structure and associated pressure regime is to generate surface wind patterns that influence changes in convective precipitation as well as temperature. While there are no appreciable changes in large-scale stable precipitation, convective precipitation changes significantly. Along the southern coast of Alaska in DJF, surface winds in NEWVT are onshore, vs. offshore in the NEWVOLDT case (Fig. 8A,B). The increase in onshore winds brings moisture-laden air off the North Pacific. When this air reaches the coastal mountains of Alaska, the moisture is dropped as convective precipitation. Over southern Alaska in DJF, there is a 20% increase in convective clouds and a 6 mm/day precipitation increase (Fig. 9A). Increased DJF convective precipitation is also seen over the west coast of North America where subtropical air is forced northward along the western mountain front instead of moving zonally across the low mountains of NEWVOLDT (Fig. 8A,B). As the subtropical air moves north and east, it rises and cools, and, as a result, convective precipitation increases (Fig. 9A).

Convective precipitation changes due to alteration of the surface wind patterns are much more pronounced in JJA. Reduced onshore flow from Tethys over the proto Himalayas (Fig. 8C,D) results in a significant decrease in convective precipitation of 7–9 mm/day over this region (Fig. 9B).

One of the most significant results of this sensitivity study is seen along the proto Front Ranges of North America. Climatic changes in this area are particularly important because this is the region where most of our proxy data are located (e.g. Greenwood and Wing, 1995). With the new topography, JJA precipitation increases significantly (by 3–5 mm/day) in this region for a total summer rainfall of 6–8 mm/day (not shown). All of this summer precipitation (6–8 mm/day) is in the form of convective precipitation. In this region, enhanced southerly surface winds off the Mississippi embayment collide with enhanced northerlies off the Arctic Ocean (Fig. 8D). These enhanced surface winds are driven by rising air over the North American Cordillera and there is a strong increase in easterly winds over this region (Fig. 8D). When the cool, dry, Arctic air meets the warm, moist, Mississippi embayment air, the result is a 40% increase in convective cloudiness and a corresponding increase in convective precipitation. These regional changes in convective precipitation may explain the much greater development of coals in basins east of the proto Front Ranges (Powder River and Hanna Basins) compared with those to the west (Bighorn and Green River Basins). It is possible that summer precipitation was greater east of the mountains due to elevation effects. The greater precipitation would have promoted formation of vegetation rich swamps and lead to greater coal production. If so, we speculate that fossils preserved in the coals of the Hanna and Powder River Basins would, therefore, reflect a wetter climate than plant fossils from the Bighorn and Green River Basins.

6.3. Climate sensitivity to changes in shorelines

We believe that one of the main controls on the amount of convective precipitation received by the proto Front Ranges is the extent of the Mississippi embayment. To test this hypothesis, a third sensitivity study, designated EMB, was conducted. The boundary conditions for EMB are identical to those of NEWVT with the exception that the Mississippi embayment has been adjusted to approximately its

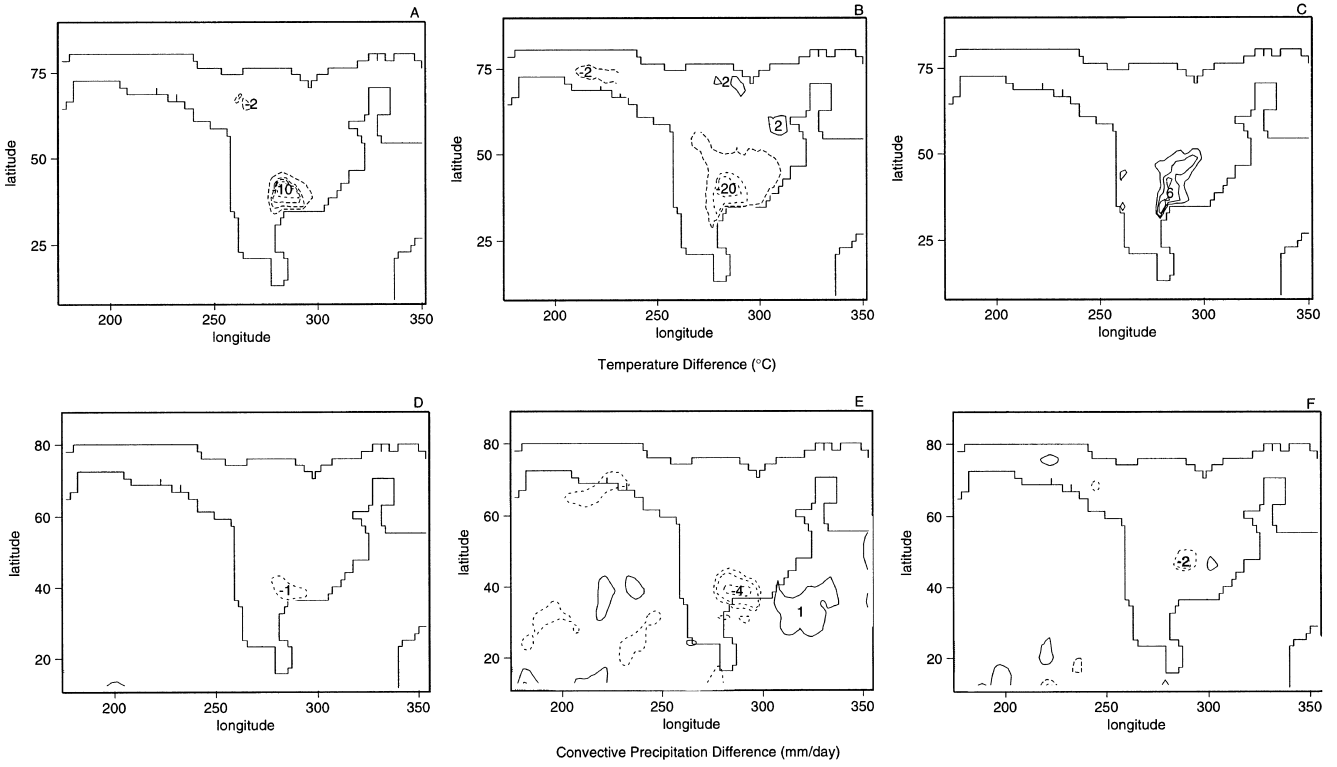

Fig. 12. (A) MAT difference over North America, EMB minus NEWVT, contours from −14°C to 14°C at 2°C, no zero contour. (B) DJF surface temperature difference over North America, EMB minus NEWVT, contours at −28°C, −20°C, −10°C, −2°C, and 2°C. (C) JJA surface temperature difference over North America, EMB minus NEWVT, contours from −6°C to 8°C at 2°C, no zero contour. (D) Mean annual convective precipitation difference over North America, EMB minus NEWVT, contours at −1 and 1 mm/day. (E) DJF convective precipitation difference over North America, EMB minus NEWVT, contours at −4, −2, −1, 1, 2, and 4 mm/day. (F) JJA convective precipitation difference over North America, EMB minus NEWVT, contours at −4, −2, −1, 1, 2, and 4 mm/day. All contoured differences presented in this plot are significant to the 99% confidence level. Significance was calculated using Chervin and Schneider's *t*-test (Chervin and Schneider, 1976a,b).

modern extent. The EMB case was started from year 8 of NEWVT and run for 5 years. Results from the last 3 years of the run were averaged together for analyses.

7. Discussion of EMB results

Changes in surface temperatures over the area previously occupied by the Mississippi embayment are the result of altering this area from ocean to land. During the winter months, land is substantially cooler than ocean, and in the summer, land warms more than the ocean does (Fig. 12B,C). Overall, the extreme cooling of the land surface (relative to the sea surface) in the winter dominates the annual signal. The result is a MAT for this region that is cooler (~ 10°C) than in the NEWVT case (Fig. 12A).

Cooler DJF temperatures along the Cordilleran Front and into the Canadian Rockies are the result of changes in the surface wind patterns (not shown). Weakened westerly flow into northern Canada in the EMB case decreases the transport of warm, moist air from the North Pacific to the interior of North America. As a result, surface temperatures in this area are reduced.

The differences in mean annual, DJF, and JJA total (not shown) and convective (Fig. 12D,E,F) precipitation over south central North America are identical. Precipitation differences are, therefore, wholly attributable to changes in convective precipitation. The DJF convective precipitation change is centered over the area that was converted from sea to land and is interpreted to be a direct effect of this conversion. The changes in JJA convective precipitation are related more to subtle alterations in atmospheric circulation and proximity to a moisture source. The hook-shaped band of decreased precipitation over central North America (Fig. 12F) is adjacent to areas just inland of the NEWVT Mississippi embayment. Infilling the Mississippi embayment to approximately its present extent in the EMB case moved the moisture source farther away from these regions; it also weakened southwesterly flow off of the embayment (not shown). Increased distance from the moisture source results in more moisture precipitating out of air masses before they reach the Laramide foreland. A decrease in wind strength reduces inland penetration of moisture-laden air off the proto Gulf of Mexico. This combination results in an overall decrease in summer precipitation in the foreland region of the Laramide uplifts; yet, summer precipitation in this area remains 5–6 mm/day. Removing the proximal moisture source slightly decreases the amount of monsoonal convective precipitation; however, the North American summer monsoon is still a robust feature.

8. Conclusions

Overall, this series of sensitivity studies indicates that relatively small (on a global scale) changes to the land surface, specifically topography, orography, and the global distribution of vegetation, have little effect on global mean climate. However, changes to the land surface have significant climatic effects at the regional scale. Indeed, the only really "global" signal, enhanced ridge and trough structure in the upper atmosphere, is significant for its influence on surface winds that help initiate, or shut down, regional monsoonal circulations.

Changes in monsoonal circulation affect regional moisture budgets. Changes in elevation affect regional surface temperature, and changes in plant LAI influence evapotranspiration in some areas. Infilling the Mississippi embayment to approximately its present extent results in increased seasonality in that region (warmer summers and cooler winters) and slightly decreases the amount of summer monsoonal precipitation over the Laramide foreland.

These model-produced regional climate responses to changes in the land surface are important because proxy data-derived estimates of paleoclimate reflect the regional climates in which those data existed. If we hope to better correlate climate model output and proxy data-derived estimates of paleoclimate, we must be able to more completely and accurately model climate responses to changes in the land surface. The magnitude of our model-produced regional climate responses indicates that a more accurate global vegetation distribution and a more realistic topography have significant effects on regional climates. Consequently, we conclude that the inclusion of more realistic boundary conditions is necessary if we wish to produce a more realistic representation of paleoclimate with a GCM.

Acknowledgements

LCS thanks the National Science Foundation (NSF) and the David and Lucile Packard Foundation for funding in support of this research. JOS thanks the Department of Defense (DOD) for fellowship support (NDESG Fellowship). Computing was carried out at the National Center for Atmospheric Research, which was funded by NSF.

References

Allmendinger, R.W., Jordan, T.E., Kay, S.M., an Isacks, B.L., 1997. The evolution of the Altiplano-Puna plateau of the Central Andes. Annu. Rev. Earth Planet. Sci. 25, 139–174.

Bonan, G.B., Pollard, D., Thompson, S.L., 1992. Effects of boreal forest vegetation on global climate. Nature 359, 716–718.

Broccoli, A.J., Manabe, S., 1992. The effects of orography on midlatitude Northern Hemisphere dry climates. J. Clim. 5, 1181–1201.

Chervin, R.M., Schneider, S.H., 1976a. A study of the response of NCAR GCM climatological statistics to random perturbations: estimating noise levels. J. Atmos. Sci. 33, 391–404.

Chervin, R.M., Schneider, S.H., 1976b. On determining the statistical significance of climate experiments with general circulation models. J. Atmos. Sci. 33, 405–412.

Chorowicz, J., Collet, B., Boravia, F.F., Mohr, P., Parrot, J.F., Korme, T., 1998. The Tana Basin, Ethiopia: intra-plateau uplift, rifting and subsidence. Tectonophysics 295, 351–367.

Crowley, T.J., Baum, S.K., 1997. Effect of vegetation on and ice-age climate model simulation. J. Geophys. Res. 102, 16463–16480.

Demko, T.M., Dubiel, R.F., Parrish, J.I., 1998. Plant taphonomy in incised valleys: implications for interpreting paleoclimate from fossil plants. Geology 26, 1119–1122.

Dettman, D.L., Lohmann, K.C., 1993. Seasonal change in Paleogene surface water $\delta^{18}O$: fresh-water bivalves of western North America. Climate Change in Continental Isotopic Records. Geophys. Monogr., vol. 78. America Geophysical Union, pp. 153–163.

Dettman, D.L., Lohmann, K.C., 2000. Oxygen isotope evidence for high-altitude snow in the Laramide Rocky Mountains of North America during the Late Cretaceous and Paleogene. Geology 28, 243–246.

Dorman, J.L., Sellers, P.J., 1989. A global climatology of albedo, roughness length and stomatal resistance for atmospheric general circulation models as represented by the Simple Biosphere Model (SiB). J. Appl. Meteorol. 28, 833–855.

Fitzgerald, P.G., 1994. Thermochronologic constraints on post-Paleozoic tectonic evolution of the central Transantarctic Mountains, Antarctica. Tectonics 13, 818–836.

Foley, J.A., Kutzbach, J.E., Coe, M.T., Levis, S., 1994. Feedbacks between climate and boreal forests during the Holocene epoch. Nature 371, 52–54.

Gebka, M., Mosbrugger, V., Schilling, H.-D., Utescher, T., 1999. Regional-scale palaeoclimate modelling on soft proxy-data basis — an example from the Upper Miocene of the Lower Rhine Embayment. Palaeogeogr., Palaeoclimatol., Palaeoecol. 152, 225–258.

Greenwood, D.R., 1992. Taphonomic constraints on foliar physiognomic interpretations of Late Cretaceous and Tertiary palaeoclimates. Rev. Palaeobot. Palynol. 71, 149–190.

Greenwood, D.R., Wing, S.L., 1995. Eocene continental climates and latitudinal temperature gradients. Geology 23, 1044–1048.

Gurnis, M., Muller, R.D., Moresi, L., 1998. Cretaceous vertical motion of Australia and the Australian–Antarctic Discordance. Science 279, 1499–1504.

Henderson-Sellers, A., Dickinson, R.E., Durbidge, T.B., Kennedy, P.J., McGuffie, K., Pitman, A.J., 1993. Tropical deforestation: modeling local- to regional-scale climate change. J. Geophys. Res. 98, 7289–7315.

Kutzbach, J.E., Gallimore, R.G., 1989. Pangaean climates: megamonsoons of the megacontinent. J. Geophys. Res. 94, 3341–3357.

Kutzbach, J.E., Prell, W.L., Ruddiman, Wm.F., 1993. Sensitivity of Eurasian climate to surface uplift of the Tibetan Plateau. J. Geol. 101, 177–190.

Lamb, S., Hoke, L., 1997. Origin of the high plateau in the Central Andes, Bolivia, South America. Tectonics 16, 623–649.

Maxson, J., Tikoff, B., 1996. Hit and run collision model for the Laramide orogeny, western United States. Geology 24, 968–972.

Molnar, P., Tapponier, P., 1975. Cenozoic tectonics of Asia: effects of a continental collision. Science 189, 419–426.

Molnar, P., Burchfield, B.C., Ziyun, Z., K'uangyi, L., Shuji, W., Minmin, H., 1987. Geologic evolution of Northern Tibet: results of an expedition to Ulugh Muztagh. Science 235, 299–305.

Norris, R.D., Jones, L.S., Corfield, R.M., Cartlidge, J.E., 1996. Skiing in the Eocene Uinta Mountains? Isotopic evidence in the Green River Formation for snow melt and large mountains. Geology 24, 403–406.

Plaziat, J.C., 1981. Late Cretaceous to Late Eocene palaeogeographic evolution of southwest Europe. Palaeogeogr., Palaeoclimatol., Palaeoecol. 36, 263–320.

Pollard, D., Thompson, S.L., 1995. Use of a land-surface transfer scheme (LSX) in a global climate model: the response to doubling stomatal resistance. Global Planet. Change 10, 129–161.

Reichert, B.K., Bengtsson, L., Åkesson, O., 1999. A statistical modeling approach for the simulation of local paleoclimatic proxy records using general circulation model output. J. Geophys. Res. 104, 19071–19083.

Roehler, H.W., 1993. Eocene climates, depositional environments, and geography, greater Green River Basin, Wyoming, Utah, and Colorado. U.S. Geol. Surv. Prof. Pap. vol. 1506-F. United States Government Printing Office, Washington, DC, pp. F1–F74.

Ruddiman, W.F., Prell, W.L., 1997. Introduction to the uplift-climate connection. In: Ruddiman, W.F. (Ed.), Tectonic Uplift and Climate Change. Plenum, New York, NY, pp. 3–15.

Rull, V., 1999. Palaeoflorisitc and palaeovegetational changes across the Paleocene/Eocene boundary in northern South America. Rev. Palaeobot. Palynol. 107, 83–95.

Sailor, D.J., Li, X., 1999. A semiempirical downscaling approach for predicting regional temperature impacts associated with climatic change. J. Clim. 12, 103–114.

Scotese, C.R., Gahagan, L.M., Larson, R.L., 1988. Plate tectonic reconstructions of the Cretaceous and Cenozoic ocean basins. Tectonophysics 155, 27–48.

Sloan, L.C., Barron, E.J., 1992. Paleogene climatic evolution: a climate model investigation of the influence of continental elevation and sea-surface temperature upon continental climate. In: Prothero, D.R., Berggren, W.A. (Eds.), Eocene–Oligocene climatic and biotic evolution. Princeton University Press, Princeton, NJ, pp. 202–217.

Sloan, L.C., Rea, D.K., 1995. Atmospheric carbon dioxide and Early Eocene climate: a general circulation modeling sensitivity study. Palaeogeogr., Palaeoclimatol., Palaeoecol. 119, 275–292.

Sloan, L.C., Pollard, D., 1998. Polar stratospheric clouds: a high latitude warming mechanism in an ancient greenhouse world. Geophys. Res. Lett. 25, 3517–3520.

Sloan, L.C., Crowley, T.J., Huber, M., Sewall, J.O., Baum, S.K., Ewing, A. Palaeogeogr., Palaeoclimatol., Palaeoecol., in review.

Tapponier, P., Molnar, P., 1979. Active faulting and Cenozoic tectonics of the Tien Shan. J. Geophys. Res. 84, 3425–3459.

Taylor, G., Truswell, E.M., McQueen, K.G., Brown, M.C., 1990. Early Tertiary palaeogeography, landform evolution, and palaeoclimates of the Southern Monaro, N.S.W., Australia. Palaeogeogr., Palaeoclimatol., Palaeoecol. 78, 109–134.

Thompson, S.L., Pollard, D., 1997. Greenland and Antarctic mass balances for present and coupled atmospheric CO_2 from the GENESIS Version-2 global climate model. J. Clim. 10, 871–900.

Wilby, R.L., Wigley, T.M.L., Conway, D., Jones, P.D., Hewitson, B.C., Main, J., Wilks, D.S., 1998. Statistical downscaling of general circulation model output: a comparison of methods. Water Resour. Res. 34, 2995–3008.

Wilf, P., 2000. Late Paleocene–Early Eocene climate changes in southwestern Wyoming: paleobotanical analysis. Geol. Soc. Am. Bull. 112, 292–307.

Wing, S.L., 1998a. Late Paleocene–Early Eocene floral and climatic change in the Bighorn Basin, Wyoming. In: Berggren, W., Aubrey, M.-P., Lucas, S. (Eds.), Late Paleocene–Early Eocene biotic and climatic events. Columbia University Press, New York, NY, pp. 371–391.

Wing, S.L., 1998b. Tertiary vegetation of North America as a context for mammalian evolution. In: Janis, C.M., Scott, K.M., Jacobs, L.L. (Eds.), Evolution of Tertiary Mammals of North America. Terrestrial Carnivores, Ungulates, and Ungulatelike Mammals, vol. 1. Cambridge Univ. Press, Cambridge, pp. 37–60.

Wing, S.L., Greenwood, D.R., 1993. Fossils and fossil climate: the case for equable continental interiors in the Eocene. Philos. Trans. R. Soc. London 341, 243–252.